PCCP

PAPER

View Article Online
View Journal | View Issue

Cite this: *Phys. Chem. Chem. Phys.*, 2014, **16**, 3798

Weak hydrogen bonding motifs of ethylamino neurotransmitter radical cations in a hydrophobic environment: infrared spectra of tryptamine$^+$–$(N_2)_n$ clusters ($n \leq 6$)

Kenji Sakota,[a] Markus Schütz,[b] Matthias Schmies,[b] Raphael Moritz,[b] Aude Bouchet,[b] Takamasa Ikeda,[a] Yuuki Kouno,[a] Hiroshi Sekiya*[a] and Otto Dopfer*[b]

Size-selected clusters of the tryptamine cation with N_2 ligands, TRA^+–$(N_2)_n$ with n = 1–6, are investigated by infrared photodissociation (IRPD) spectroscopy in the hydride stretch range and quantum chemical calculations at the ωB97X-D/cc-pVTZ level to characterize the microsolvation of this prototypical aromatic ethylamino neurotransmitter radical cation in a nonpolar solvent. Two types of structural isomers exhibiting different interaction motifs are identified for the TRA^+–N_2 dimer, namely the TRA^+–N_2(H) global minimum, in which N_2 forms a linear hydrogen bond (H-bond) to the indolic NH group, and the less stable TRA^+–N_2(π) local minima, in which N_2 binds to the aromatic π electron system of the indolic pyrrole ring. The IRPD spectrum of TRA^+–$(N_2)_2$ is consistent with contributions from two structural H-bound isomers with similar calculated stabilization energies. The first isomer, denoted as TRA^+–$(N_2)_2$(2H), exhibits an asymmetric bifurcated planar H-bonding motif, in which both N_2 ligands are attached to the indolic NH group in the aromatic plane *via* H-bonding and charge–quadrupole interactions. The second isomer, denoted as TRA^+–$(N_2)_2$(H/π), has a single and nearly linear H-bond of the first N_2 ligand to the indolic NH group, whereas the second ligand is π-bonded to the pyrrole ring. The natural bond orbital analysis of TRA^+–$(N_2)_2$ reveals that the total stability of these types of clusters is not only controlled by the local H-bond strengths between the indolic NH group and the N_2 ligands but also by a subtle balance between various contributing intermolecular interactions, including local H-bonds, charge–quadrupole and induction interactions, dispersion, and exchange repulsion. The systematic spectral shifts as a function of cluster size suggest that the larger TRA^+–$(N_2)_n$ clusters with n = 3–6 are composed of the strongly bound TRA^+–$(N_2)_2$(2H) core ion to which further N_2 ligands are weakly attached to either the π electron system or the indolic NH proton by stacking and charge–quadrupole forces.

Received 30th September 2013,
Accepted 9th December 2013

DOI: 10.1039/c3cp54127d

www.rsc.org/pccp

1. Introduction

Biological processes in a living cell, such as molecular recognition, protein folding, and catalytic biochemical reactions, are largely controlled by the interactions of biomolecular structures with water.[1,2] On the other hand, many biomolecules and biopolymers, such as proteins and phospholipids, contain hydrophobic parts which avoid interactions with water. In some cases, such hydrophobic parts induce entropic forces as well as dispersion forces, leading to precise molecular recognition and protein folding.[3,4] Usually, the hydrophobic parts are in the interior of biological macromolecules to prevent interactions with water. In such hydrophobic parts, weak hydrogen bonds (H-bonds), in which water is not involved, are formed to stabilize the structures of the biological macromolecules.[5] Therefore, weak H-bonds, such as C–H···O and C–H···π interactions, are important to understand the noncovalent interactions in biomolecular assemblies.

Conventional H-bonding interactions between the electropositive H atom and electronegative atoms, such as O–H···O and N–H···N H-bonds, have extensively been investigated using various spectroscopic techniques. Although weak H-bonds have much smaller interaction energies than conventional H-bonds, the sum of many weak H-bonds can be significant and decisive in regulating the shape and reactivity of biological macromolecules.[5] The determination of the local H-bonding structure around a substrate offers essential information for understanding the detailed mechanisms of biological processes at the molecular level. Laser spectroscopy of cold and size-selected clusters

[a] *Department of Chemistry, Faculty of Sciences, and Department of Molecular Chemistry, Graduate School of Sciences, Kyushu University, 6-10-1 Hakozaki, Higashi-ku, Fukuoka 812-8581, Japan. E-mail: sekiya@chem.kyushu-univ.jp*
[b] *Institut für Optik und Atomare Physik, Technische Universität Berlin, D-10623 Berlin, Germany. E-mail: dopfer@physik.tu-berlin.de*

generated in a supersonic expansion is an ideal tool to directly probe local H-bonding structures by eliminating thermal and environmental effects which give rise to spectral complexity.[6–16] The combination with mass spectrometric techniques allows for the investigation of the effect of stepwise solvation on the structure of the H-bonded network.

Here, we report infrared photodissociation (IRPD) spectra and quantum chemical calculations of mass-selected clusters of the tryptamine (TRA) cation microsolvated by a controlled number of nitrogen molecules, $TRA^+–(N_2)_n$ with n = 1–6, to characterize the microsolvation of this prototypical ethylamino neurotransmitter radical cation in a nonpolar solvent. This cluster system has been chosen for the following reasons. TRA belongs to the family of aromatic ethylamino neurotransmitters and is an analogue of serotonin and the amino acid tryptophan. The flexible ethylamino side chain attached to the indole chromophore gives rise to several low-energy conformers of TRA. These conformers and their H-bonding interaction with water have been investigated in detail.[17–31] Seven stable conformers of neutral TRA in the S_0 ground electronic state are observed under supersonic jet conditions.[17] IR spectroscopy combined with quantum chemical calculations has revealed that the predominant TRA conformer in S_0 is G*py*(out), which has a *gauche* conformation with the side chain oriented toward the pyrrole side of indole and the lone pair of the amino group pointing away from indole (see ref. 17 for the notation of the isomers of TRA). The potential energy barriers between the various TRA conformers have been determined using stimulation emission pumping-population transfer spectroscopy.[18] In the S_0 state of TRA–H_2O, however, only a single conformer, G*py*(out), is observed.[19,20] This result implies that the seven conformers of isolated TRA collapse into a single conformer in TRA–H_2O by conformational locking induced by a single H-bonded water ligand.[20] Gu and Knee reported the zero kinetic energy (ZEKE) photoelectron spectra of TRA and the photoionization efficiency (PIE) and fragmentation spectra of $TRA^+–H_2O$.[21] They measured the ZEKE and PIE spectra of six conformers of TRA. The most stable G*py*(out) conformer of neutral TRA does not show a resolved ZEKE spectrum. Moreover, its PIE spectrum obtained through the S_1 origin shows only a broad unstructured onset, suggesting that the conformation of its ethylamino side chain drastically changes upon photoionization. In addition, they suggested a substantial rearrangement of the intermolecular H-bond in the cationic D_0 ground electronic state of $TRA^+–H_2O$ upon photoionization based on their spectroscopic results combined with quantum chemical calculations.[21] However, no direct experimental evidence for the details of the structural rearrangement was obtained. Very recently, we reported the IR spectrum of $TRA^+–H_2O$ generated by resonant photoionization,[22] which proved that the water molecule indeed transfers from the ethylamino group to the indolic NH group upon photoionization into the D_0 state. The minimum energy pathway of this photoionization-induced rearrangement of the H-bonding motif was also determined by intrinsic reaction coordinate calculations.

In contrast to water, no information is available for the weak interaction of TRA^+ with nonpolar ligands. Thus, the current study of $TRA^+–(N_2)_n$ provides a first impression of the microsolvation of this prototypical aromatic neurotransmitter cation in a nonpolar solvent. As TRA^+ is expected to form weak H-bonds with nonpolar N_2 molecules, their characteristic features become accessible by direct comparison with the strong conventional H-bond observed in $TRA^+–H_2O$. The current $TRA^+–(N_2)_n$ study extends our previous characterization of $A^+–(N_2)_n$ clusters with more simple aromatic chromophores (A^+),[32] such as benzene,[33,34] phenols and naphthols,[35–39] anilines,[40–42] imidazole,[43] cyclopropenyl,[44,45] and indole (In).[46] These studies revealed that the microsolvation process of acidic aromatic ions in molecular nitrogen is dominated by the competition between two principal binding motifs, namely H-bonding to the acidic functional OH and NH groups and π-stacking to the aromatic ring. In this respect, comparison between $In^+–(N_2)_n$ and $TRA^+–(N_2)_n$ will directly reveal the effects of the ethylamino side chain on the intermolecular interaction, with respect to both the acidity of the indolic NH group and the sequential cluster growth. The weak H-bonds in $In^+–(N_2)_n$ clusters with $n \leq 8$ have been investigated previously.[46] For $In^+–N_2$, two stable isomers, namely the H-bound and π-bound structures, are identified, in which N_2 is either H-bonded to the NH group (global minimum) or attached to the aromatic π-electron system, respectively. While in the H-bonded $In^+–N_2$ dimer, the N_2 ligand binds linearly to the NH group, in the larger $In^+–(N_2)_n$ clusters two N_2 molecules are H-bonded to the NH group in the aromatic plane leading to a bifurcated double H-bonded motif, and additional N_2 ligands are attached to the aromatic ring of In^+. Comparison of the open-shell TRA^+ radical cation with previous studies on protonated closed-shell aromatic ethylamino neurotransmitters (*e.g.*, serotonin, dopamine, histamine)[47–49] will reveal the effects of the charge distribution on the orientation of the side chain and the intramolecular NH–π interaction. The present study provides a detailed analysis of the IRPD spectra of $TRA^+–(N_2)_n$ (n = 1–6) with quantum chemical calculations including a natural bond orbital (NBO) analysis to obtain insights into the intermolecular interactions acting on this prototypical aromatic neurotransmitter cation in a nonpolar environment.

2. Experimental and computational methods

IRPD spectra of mass-selected $TRA^+–(N_2)_n$ cluster ions are recorded in a tandem quadrupole mass spectrometer coupled to an electron impact ionization source and an octopole ion trap.[13,32,50] Cold $TRA^+–(N_2)_n$ clusters are produced in a pulsed supersonic expansion by electron and/or chemical ionization of TRA close to the nozzle orifice and subsequent clustering reactions. The expanding gas mixture is produced by passing N_2 carrier gas (5 bar) through a reservoir filled with TRA heated to 410 K. A typical mass spectrum of the ion source is shown in Fig. 1 for the mass range 20–195 u. It is dominated by $X^+–(N_2)_n$ cluster series with $X^+ = N_2^+$, N_3^+, and H_2O^+, and weaker signals arising from TRA^+ and its N_2 clusters. The abundance of $TRA^+–(N_2)_n$ decreases rapidly with increasing cluster size, consistent with the formation of

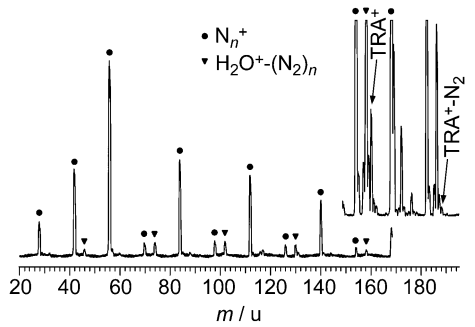

Fig. 1 Mass spectrum of the electron impact ion source obtained from the expansion of tryptamine vapor ($T \sim 410$ K) seeded in 5 bar N_2. A vertically expanded mass spectrum is also shown to indicate weak peaks. TRA^+ and TRA^+–N_2 are observed at m = 160 and 188 u, respectively. Major cluster series, N_n^+ and H_2O^+–$(N_2)_n$, are indicated by filled circles and triangles, respectively.

weakly-bound clusters by sequential addition of N_2 ligands to the TRA^+ ion. TRA^+–$(N_2)_n$ ions of interest are mass selected by the first quadrupole and irradiated in an adjacent octopole with a tuneable IR laser pulse (ν_{IR}) generated by an optical parametric oscillator (IR-OPO) pumped using a nanosecond Q-switched Nd:YAG laser. The IR-OPO laser is characterized by a pulse energy of 2–5 mJ in the 2800–3500 cm^{-1} range, a repetition rate of 10 Hz, and a bandwidth of 1 cm^{-1}. Calibration of the IR laser frequency (ν_{IR}) accurate to better than 1 cm^{-1} is accomplished using a wavemeter. Resonant excitation into vibrational resonances induces the evaporation of N_2 ligands, according to:

$$TRA^+\text{–}(N_2)_n + h\nu_{IR} \rightarrow TRA^+\text{–}(N_2)_m + (n - m)N_2 \qquad (1)$$

The rupture of the weak intermolecular bonds is the only fragment channel observed. TRA^+–$(N_2)_m$ fragment ions are selected by the second quadrupole and monitored using a Daly detector as a function of ν_{IR} to obtain the IRPD spectra of the TRA^+–$(N_2)_n$ parent clusters. In general, laser-induced dissociation of TRA^+–$(N_2)_n$ leads to a narrow range of TRA^+–$(N_2)_m$ fragment channels (indicated as $n \rightarrow m$), and this information will be used to estimate the binding energies of the ligands.[32] To establish and confirm the composition of a given cluster ion, collision-induced dissociation (CID) spectra are recorded. For this purpose, the octopole is filled with N_2 up to 10^{-5} mbar, which results in collisions with $\sim$10 eV collision energy in the laboratory frame.

Quantum chemical calculations are performed at the ωB97X-D/cc-pVTZ level to obtain stable structures, binding energies, harmonic vibrational frequencies, IR intensities, and NBO charge distributions of TRA^+–$(N_2)_n$ with $n \leq 2$.[52] Harmonic frequencies are scaled by a factor of 0.9453, obtained by matching the experimental and calculated NH stretch frequencies of In^+ (ν_{NH} = 3454 cm^{-1}).[46,51] All binding and relative energies are corrected for vibrational zero-point energies. While the ωB97X-D/cc-pVTZ data agree semi-quantitatively with the experimental data, initial calculations at the B3LYP/cc-pVDZ, CAM-B3LYP/aug-cc-pVDZ, M06-2X/(aug-)cc-pVTZ, and ωB97X-D/cc-pVDZ levels yielded much less satisfying results. In the NBO analysis, pairs of NBOs are obtained for the α and β electrons because of the unrestricted open-shell calculations. The orbitals of α and β electrons, however, have similar shapes. Therefore, although only NBOs of the α electrons are displayed in the figures, the sum of the second order perturbative energies, $E^{(2)}_{i\rightarrow j^*}$, of α and β electrons is evaluated.

3. Results and discussion

3.1 TRA^+–N_2 dimer

Fig. 2 shows the IRPD spectra of TRA^+–$(N_2)_n$ with n = 1–6 recorded in the range of the indolic NH stretch fundamental (ν_{NH}) by monitoring the dominant TRA^+–$(N_2)_m$ fragment channel, denoted as $n \rightarrow m$. The IRPD spectrum of the TRA^+–N_2 dimer (n = 1) shows two transitions with maxima at 3395 ± 1 and 3447 ± 1 cm^{-1}, which are assigned to the ν_{NH} transitions of the H-bound and π-bound isomers, respectively, by comparison to those observed for the related In^+–N_2 isomers, with ν_{NH} = 3379 and 3450 cm^{-1} for In^+–N_2(H) and In^+–N_2(π), respectively.[46] The blue shaded band profile of the intense ν_{NH} band of the H-bound isomer, with a large width of $\sim$25 cm^{-1} and a band origin close to the P-branch head, is typical for the excitation of a proton donor stretch vibration and thus confirms the isomer assignment.[32,37,53–55]

The computed structures of the relevant TRA^+–N_2 isomers are illustrated in Fig. 3, and important parameters are listed in Table 1. In TRA^+–N_2(H), the N_2 molecule is linearly H-bonded to the indolic NH group, whereas it is attached to the aromatic pyrrole ring of TRA^+ in TRA^+–$N_2(\pi_{top})$ and TRA^+–$N_2(\pi_{bottom})$. All attempts to optimize π-bound structures with N_2 binding to the phenyl ring converged to those with N_2 attached to the

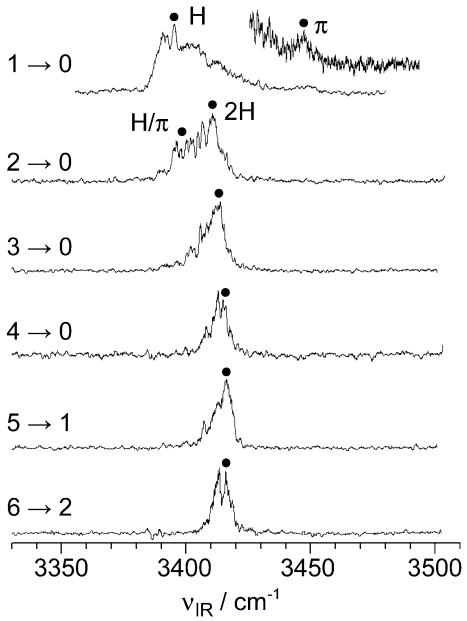

Fig. 2 IRPD spectra of TRA^+–$(N_2)TRA^+$–$(N_2)_n$ (n = 1–6) obtained by monitoring the TRA^+–$(N_2)_m$ fragment channels (indicated as $n \rightarrow m$). The vibrational bands are assigned to the indolic NH stretching fundamental (ν_{NH}). The IRPD spectra of TRA^+–$(N_2)_n$ (n = 1–6) recorded at higher sensitivity is also shown. The vibrational frequencies marked with filled circles are plotted in Fig. 7.

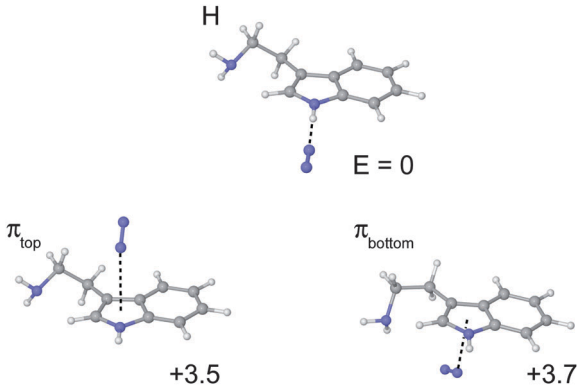

Fig. 3 Structures of the H-bonded $TRA^+–N_2(H)$ global minimum and π-bound $TRA^+–N_2(\pi)$ local minima obtained at the ωB97X-D/cc-pVTZ level. Relative stabilization energies are given in kJ mol^{-1}.

pyrrole ring. The binding energy of $TRA^+–N_2(H)$, D_0 = 11.7 kJ mol^{-1}, is higher by 3.5 and 3.7 kJ mol^{-1} than those of $TRA^+–N_2(\pi_{top})$ and $TRA^+–N_2(\pi_{bottom})$, respectively. The H-bonded ν_{NH} band in the IRPD spectrum of $TRA^+–N_2$ is readily assigned to the global minimum structure in Fig. 3. The calculations predict very similar ν_{NH} frequencies and IR intensities for $TRA^+–N_2(\pi_{top})$ and $TRA^+–N_2(\pi_{bottom})$. As the difference of the binding energies of $TRA^+–N_2(\pi_{top})$ and $TRA^+–N_2(\pi_{bottom})$ is small (0.2 kJ mol^{-1}), we assign the free ν_{NH} band observed in the IRPD spectrum to both π-bound isomers.

For completeness, we note that the exact position of the non H-bonded N_2 ligand can in fact not be derived from the experimental IRPD spectrum. The only experimental information derived from the small or vanishing ν_{NH} frequency shift (*vide infra*) is that the N_2 ligand does not occupy a H-bonded position. Comparison with related aromatic complexes[32] as well as the current computational studies reveal, however, that the π-binding sites are by far the most stable non H-bonding sites in this type of clusters and thus the favoured assignment. Using the ratios of the integrated band intensities (~20) and the calculated IR oscillator strengths of ν_{NH} of the H-bound and π-bound isomers of $TRA^+–N_2$ (~3.5), their relative abundance in the expansion can be estimated and an upper limit of ~15% is derived for the population of the π-bound isomers under the present experimental conditions. As previous studies demonstrated that the electron impact source mainly produces the most stable isomer of a given cluster ion, this result clearly indicates that the H-bound isomer is the global minimum, whereas the π-bound dimers are less stable local minima. This conclusion is further supported by the IRPD spectra of larger $TRA^+–(N_2)_n$ clusters and the quantum chemical calculations.

The different orientations of the flexible ethylamino side chain of TRA^+ give rise to several low-energy conformers (Fig. 4). In principle, the symmetric and antisymmetric NH stretch vibrations of the amino group in the side chain contain information about its orientation. Unfortunately, these vibrations are too weak to be detected in the IRPD spectra of $TRA^+–(N_2)_n$ in Fig. 2. The theoretical search for stable structures of TRA^+ predicts the G*py*(in) isomer shown in Fig. 4 as the most stable one at the ωB97X-D/cc-pVTZ level. Seven stable conformers in the S_0 state have been identified in the $S_1–S_0$ excitation spectrum of TRA. Gu and Knee reported the ZEKE and PIE spectra of TRA obtained *via* the S_1 origins of each neutral conformer.[21] The most stable conformer in the S_0 state, G*py*(out), shows a broad onset in the PIE spectrum, implying a large structural change upon photoionization. DFT calculations at the M06-2X/aug-cc-pVDZ level for stable conformers in the S_0 and D_0 states predict that G*py*(out) in the S_0 state isomerizes toward the most stable G*py*(in) conformer in the D_0 state involving a large conformational change. This result is consistent with the observation of the broad onset in the PIE spectrum and the unresolved ZEKE spectrum of G*py*(out). Thus, all available experimental and computational data are consistent with G*py*(in) being the most stable conformer in the D_0 state. In this work, cationic species are produced by electron ionization, which preferentially generates the most stable conformer in a supersonic expansion. Based on the previous work[21] and our DFT calculations (Fig. 4), we assume as a working hypothesis that $TRA^+–(N_2)_n$ with n = 1–6 also have the same orientation of the ethylamino side chain as G*py*(in). This scenario is reasonable because the relative energies of the less stable TRA^+ isomers (4–20 kJ mol^{-1}) are large compared to typical N_2 binding energies, so that it is unlikely that N_2 complexation changes the energetic order of the most stable

Table 1 Salient parameters of the intermolecular NH–N_2 and intramolecular indolic N–H bonds of selected $TRA^+–(N_2)_n$ isomers evaluated at the ωB97X-D/cc-pVTZ level

Parameter[a]	TRA^+	$TRA^+–N_2(H)$	$TRA^+–N_2(\pi_{top})$	$TRA^+–N_2(\pi_{bottom})$	$TRA^+–N_2(2H)^d$	$TRA^+–N_2(H/\pi)^d$	$TRA^+–N_2(2\pi)^d$
R_{NH}/Å	1.00715	1.01206	1.00711	1.00705	1.01085	1.01189	1.00698
$R_{NH–N_2}$/Å		2.16	3.93	3.93	2.34/2.58	2.16/3.85	3.91/3.90
$R_{N–N_2}$/Å		3.17	3.45	3.52	3.25/3.27	3.17/3.40	3.43/3.43
$\theta_{N–H–N_2}$/deg		176.7	55.1	58.7	148.8/125.2	178.3/56.7	55.3/55.0
$\theta_{N–N–N}$/deg		178.1	156.7	108.0	173.7/177.5	179.5/149.3	150.8/155.5
ν_{NH}[b]/cm^{-1}	3457	3379 (3395)	3458 (3447)	3458 (3447)	3411 (3411)	3383 (~3400)	3457
I_{NH}/km mol^{-1}	169	616	167	169	418	608	164
D_e[c]/kJ mol^{-1}		14.2 (1188)	9.6 (806)	9.1 (763)	23.9 (1996)	24.2 (2021)	18.5 (1547)
D_0[c]/kJ mol^{-1}		11.7 (981)	8.2 (688)	8.0 (672)	19.7 (1650)	19.5 (1630)	15.3 (1275)

[a] Intramolecular N–H bond length (R_{NH}), stretch frequency and IR intensity (ν_{NH}, I_{NH}); intermolecular NH–N_2 and $N_{indole}–N_2$ bond lengths ($R_{NH–N_2}$, $R_{N–N_2}$), bond angles ($\theta_{N–H–N_2}$, $\theta_{N–N–N}$), and binding energies ($D_{e/0}$). [b] Experimental values are listed in parentheses. [c] Binding energies in cm^{-1} are listed in parentheses. [d] Numbers separated by a slash correspond to the $N_2(1)$ and $N_2(2)$ ligands (Fig. 6).

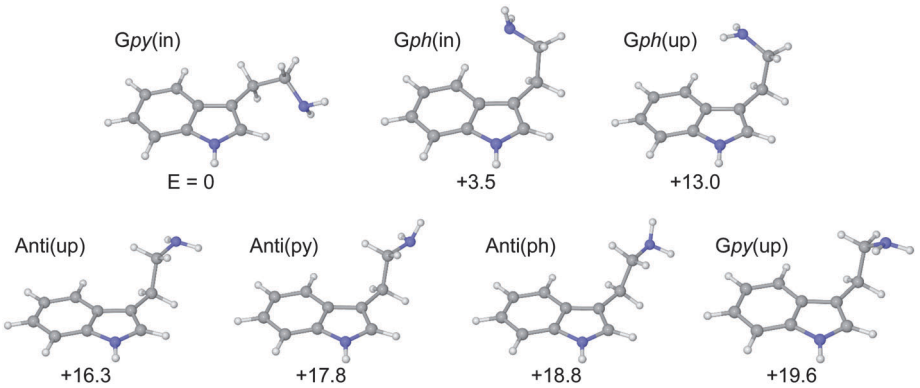

Fig. 4 Calculated structures of TRA^+ isomers with different ethylamino side chain conformations obtained at the ωB97X-D/cc-pVTZ level. Relative stabilization energies are given in kJ mol^{-1}.

TRA^+ isomer in $TRA^+–(N_2)_n$. Unfortunately, the measured IRPD spectrum in the C–H stretch range of $TRA^+–N_2$ (not shown) is also not conclusive about the exact side chain orientation, although it is consistent with the G*py*(in) configuration of TRA^+ in $TRA^+–N_2$. Significantly, the relative orientation between the ethylamino side chain and the indolic chromophore in the most stable G*py*(in) conformer of TRA^+ is very different from that in protonated serotonin,[47] in which the protonated amino group points toward the indolic ring to form an intramolecular $NH^+–\pi$ H-bond. The different structural motifs of TRA^+ and protonated serotonin arise from their different charge distributions. In TRA^+, the indolic chromophore has a substantial positive partial charge (+0.90 *e* for G*py*(in)), which prevents the proton of the amino group from interacting with the indole ring. On the other hand, the positive charge in protonated serotonin is mostly localized on the protonated amino group, which strongly favors the intramolecular $NH^+–\pi$ interaction.

Unfortunately, the ν_{NH} frequency of bare TRA^+ has not been measured yet. It is, however, well known that π-bonded N_2 ligands hardly affect the properties of the N–H and O–H bonds in aromatic molecules.[46] Therefore, ν_{NH} of the π-bound isomer is very close to that of bare TRA^+, with a minor blueshift of ≤ 5 cm^{-1}. The calculations predict shifts of + 1 cm^{-1} for both $TRA^+–N_2(\pi_{top})$ and $TRA^+–N_2(\pi_{bottom})$. Approximating ν_{NH} of TRA^+ by ν_{NH} of the π-bound isomers (3447 cm^{-1}), the ν_{NH} frequency of the $TRA^+–N_2(H)$ isomer is redshifted by −52 cm^{-1} upon complexation, being consistent with the H-bond formation between the indolic NH group and the N_2 ligand. The ν_{NH} frequency of $TRA^+–H_2O(H)$ is observed at 3178 cm^{-1},[22] which corresponds to a much larger redshift of −269 cm^{-1} than for $TRA^+–N_2(H)$. Thus, the H-bond in $TRA^+–N_2(H)$ is much weaker than in $TRA^+–H_2O(H)$, which has a strong conventional N–H···O H-bond with D_0 = 57.8 kJ mol^{-1}.

3.2 $TRA^+–(N_2)_2$ trimer

Fig. 5 compares the IRPD spectrum of $TRA^+–(N_2)_2$ in the ν_{NH} range with the predicted ν_{NH} transitions of the H/π, 2H, and 2π isomers, where the notation *x*H/*y*π designates $TRA^+–(N_2)_2$ isomers with *x* H-bound and *y* π-bound ligands. Their computed structures are illustrated in Fig. 6, and important parameters

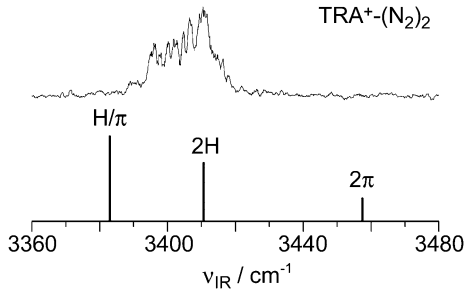

Fig. 5 IRPD spectrum of $TRA^+–(N_2)_2$ in the vicinity of the indolic NH stretch fundamental (ν_{NH}) compared to the ν_{NH} frequencies of the H/π, 2H, and 2π isomers (Fig. 6) predicted at the ωB97X-D/cc-pVTZ level.

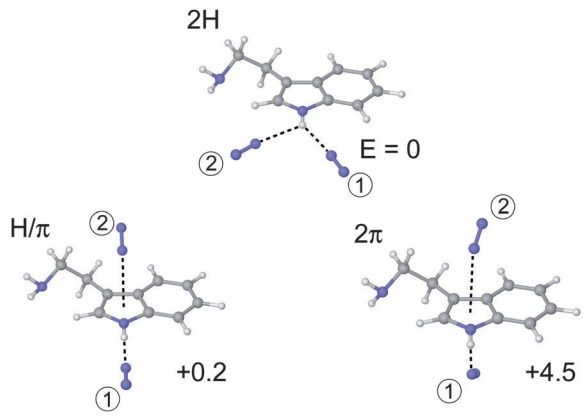

Fig. 6 Calculated structures of the 2H, H/π, and 2π isomers of $TRA^+–(N_2)_2$ obtained at the ωB97X-D/cc-pVTZ level. Relative stabilization energies are given in kJ mol^{-1}. The circled numbers are the labels of each N_2 molecule.

are listed in Table 1. The theoretical IR spectra predict that two out of the three stable isomers, namely H/π and 2H, have their ν_{NH} transitions in the vicinity of the broad band observed in the IRPD spectrum. In the H/π isomer, one N_2 molecule binds linearly to the NH group and the other N_2 ligand is attached to the aromatic ring of TRA^+. The negligible interaction between the two N_2 units leads to essentially additive behavior with respect to structural and energetic properties upon sequential

complexation. On the other hand, in the 2H isomer, the two N_2 molecules are both H-bonded to the NH group in the indolic plane *via* an asymmetric bifurcated H-bond arrangement. The two H-bonds are, however, not equivalent, with the H-bond of $N_2(1)$ being stronger than that of $N_2(2)$. The very different H-bonding motifs in H/π and 2H have largely different ν_{NH} frequencies, which thus serve as sensitive indicators for their respective H-bonding arrangements.

In contrast to the blue shaded ν_{NH} band contour of the TRA^+–N_2(H) dimer (Fig. 2), the measured ν_{NH} transition of TRA^+–$(N_2)_2$ shows a red shaded profile with maximum intensity at 3411 cm^{-1} (Fig. 5). The broad and asymmetric profile suggests that more than one isomer contributes to the IRPD spectrum of TRA^+–$(N_2)_2$. By comparing the experimental and theoretical IR spectra, the red side of the measured ν_{NH} band can be assigned to the H/π isomer, whereas the blue side is attributed to the 2H isomer. The difference between the calculated binding energies of the two isomers is very small (0.2 kJ mol^{-1}), which further supports these assignments. The red side of the observed ν_{NH} band appears at around 3400 cm^{-1}, which is only slightly blueshifted by 5 cm^{-1} from that of the TRA^+–N_2(H) dimer (3395 cm^{-1}). This observation is expected because the H-bond of the $N_2(1)$ ligand in the H/π isomer is similar to that of the TRA^+–N_2(H) dimer, and the π-bonded $N_2(2)$ ligand hardly affects the H-bond to $N_2(1)$. On the other hand, the blue side of the observed ν_{NH} band in the IRPD spectrum has its maximum intensity at 3411 cm^{-1}, which corresponds to a substantial blueshift of 16 cm^{-1} from that of TRA^+–N_2(H). Hence, the local H-bond strength of the 2H isomer is smaller than that of the H/π isomer, although the binding energies of both isomers are very similar (*vide infra*). It should be noted that five or six peaks are observed in the experimental ν_{NH} spectrum of TRA^+–$(N_2)_2$, although they are currently ascribed to only two isomers. This discrepancy is due to the unresolved rotational band contours and sequence of hot band transitions of each isomer, although we cannot completely rule out that more than the two considered isomers contribute to the measured spectrum.

The indolic ν_{NH} mode of the 2π isomer of TRA^+–$(N_2)_2$ has a similar frequency (predicted to be 3457 cm^{-1}, Fig. 5) to ν_{NH} of TRA^+–N_2(π) and TRA^+, because the π-bonded N_2 ligands hardly affect the NH bond strength. The broad ν_{NH} band is observed below ~3420 cm^{-1}, indicating that the 2π isomer can be ruled out as a structural motif for the signals observed for TRA^+–$(N_2)_2$. There is no signal near 3457 cm^{-1} in the IRPD spectrum, implying that the abundance of the 2π isomer of TRA^+–$(N_2)_2$ is below the detection limit. This observation confirms the conclusions drawn from the dimer spectrum that π-bonding to the aromatic ring is much less favorable than H-bonding to the indolic NH group.

3.3 Larger TRA^+–$(N_2)_n$ clusters

The ν_{NH} frequencies extracted from the IRPD spectra of TRA^+–$(N_2)_n$ with n = 1–6 (Fig. 2) are plotted in Fig. 7 as a function of the cluster size. The ν_{NH} shifts directly reflect the preferred solvation shell structure, which begins with the solvation of the indolic NH group by two H-bonded N_2 ligands (large ν_{NH} redshift

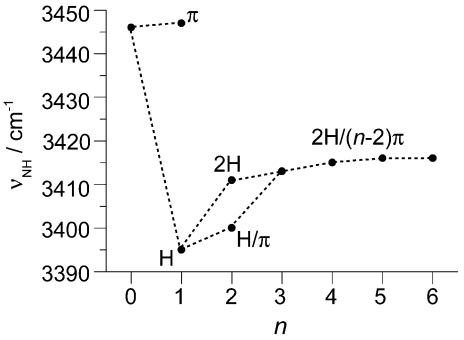

Fig. 7 Plot of the maxima of the NH stretching frequencies (ν_{NH}) in the IRPD spectra of TRA^+–$(N_2)_n$ (n = 1–6) as a function of cluster size. The ν_{NH} frequency of the TRA^+ monomer (n = 0) is estimated from ν_{NH} measured for TRA^+–N_2(π) and the computed frequency shift (1 cm^{-1}).

followed by substantial blueshift) and continues with attachment of π-bonded ligands (very small incremental blueshifts). The ν_{NH} band profiles of the n = 3–6 clusters in Fig. 2 are much narrower and more symmetric than those of $n \leq 2$ due to a drastic decrease in the band intensity on the red side. The ν_{NH} bands of n = 3–6 centered at 3413, 3415, 3416, and 3416 cm^{-1} show only minor blueshifts from ν_{NH} of the 2H isomer of the n = 2 cluster ($\lesssim$5 cm^{-1}). This observation implies that the predominant route for microsolvation of TRA^+–$(N_2)_n$ with $n \geq 3$ proceeds by attachment of weakly bound N_2 ligands to the 2H isomer of n = 2 at the aromatic ring or other weak binding sites located away from the indolic NH group. The general trend of the ν_{NH} spectral shifts of TRA^+–$(N_2)_n$ is similar to that observed previously for In^+–$(N_2)_n$,[46] indicating that the ethylamino side chain has only a minor impact on the microsolvation with N_2 in the size range considered.

3.4 Further discussion

3.4.1 NBO analysis. According to the ν_{NH} spectral shifts, the preferred H-bonding arrangement of the indolic NH group in TRA^+–$(N_2)_n$ changes with increasing solvation from the formation of a single linear H-bond for n = 1 to the planar bifurcated asymmetric double H-bonded motif for $n \geq 3$. In TRA^+–$(N_2)_2$, both types of H-bond configurations coexist with significant population, *i.e.*, the switch in the preferred H-bonding motif occurs at n = 2. To obtain further insight into the nature of these qualitatively different H-bond configurations, the NBOs are considered for the various isomers of TRA^+–$(N_2)_n$ with $n \leq 2$ and compared to those of TRA^+–H_2O (Fig. 8). In the NBO model, the interaction strength of conventional σ-type A–H···B H-bonds is correlated with the donor–acceptor charge transfer interaction from the lone pair orbital of the B atom of the H-bond acceptor to the antibonding σ* orbital of the A–H donor bond.[56,57] This charge transfer interaction is evaluated by the second-order perturbative energy, $E^{(2)}_{i\rightarrow j^*}$, where i and j^* denote the lone pair of B and the σ* orbital of the A–H bond, respectively. The $E^{(2)}_{i\rightarrow j^*}$ energies of the H, H/π, and 2H isomers of TRA^+–$(N_2)_{1,2}$ are compared in Fig. 8 with that of TRA^+–H_2O(H) to directly contrast weak and strong H-bonds of TRA^+.

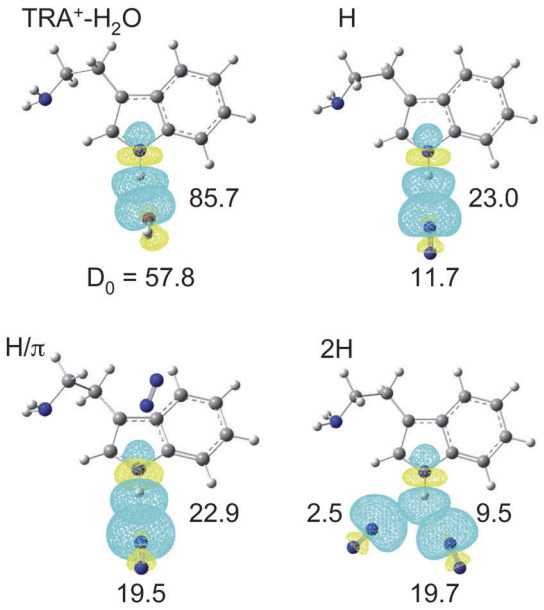

Fig. 8 Natural bond orbitals of $TRA^+–H_2O$(H), $TRA^+–N_2$(H), $TRA^+–(N_2)_2$(H/π), $TRA^+–(N_2)_2$(2H). Blue and yellow colors indicate the lone pair orbitals of the N_2 molecules and the antibonding σ* orbitals of the N–H bond, respectively, which exhibit large charge transfer interactions. The second order perturbative energies $\left(E^{(2)}_{i\rightarrow j^*}\right)$ of each local H-bond are given in kJ mol^{-1}. Binding energies (D_0) of each cluster are also given in kJ mol^{-1}.

The $E^{(2)}_{i\rightarrow j^*}$ energies of $TRA^+–(N_2)_{1,2}$ are much smaller than that of $TRA^+–H_2O$, which has a conventional N–H···O H-bond. Hence, the local H-bonds between the NH group and the N_2 molecules in $TRA^+–(N_2)_{1,2}$ are much weaker than the conventional H-bond in $TRA^+–H_2O$. The $E^{(2)}_{i\rightarrow j^*}$ values of the H and H/π isomers for n = 1 and n = 2 are very similar (23.0 and 22.9 kJ mol^{-1}), because of their similar linear H-bond architecture. For comparison, the $E^{(2)}_{i\rightarrow j^*}$ energies of the stronger and weaker H-bonds in the 2H isomer are 9.5 and 2.5 kJ mol^{-1}, respectively. Thus, even the $E^{(2)}_{i\rightarrow j^*}$ energy of the stronger H-bond is much smaller than those of the H and H/π isomers, because both H-bonds in the 2H isomer largely deviate from linearity. Furthermore, the sum of the $E^{(2)}_{i\rightarrow j^*}$ energies of the two bifurcated H-bonds (12.0 kJ mol^{-1}) in the 2H isomer is also smaller than that of the H/π isomer, consistent with the observation that ν_{NH} of the 2H isomer is blueshifted compared to that of the H/π isomer. Hence, the *local* H-bond strengths in the 2H isomer are smaller than that of the H/π isomer, although both isomers have similar binding energies (19.7 and 19.5 kJ mol^{-1}). This discrepancy is rationalized by other contributions to the intermolecular interaction, in addition to the considered H-bonds. For example, N_2 has a large electric quadrupole moment (-5×10^{-40} C m^2), so that charge–quadrupole interactions play a significant role in determining the total stabilities of the $TRA^+–(N_2)_2$ isomers. In addition, dispersion forces may contribute with different strengths, *e.g.*, for isomers with and without π-bonded ligands. Therefore, the total stability of these isomers is not only determined by the local H-bond strengths but also by a subtle balance between several types of intermolecular interactions, such as local H-bonds, charge–quadrupole, induction, dispersion, and exchange repulsion. The precise spectroscopic data along with their theoretical analysis presented in this study may contribute to a deeper understanding of the weak H-bonding interactions, which play an important role in biological systems.

3.4.2 Ligand binding energies. The photofragmentation branching ratios observed upon IRPD of larger $TRA^+–(N_2)_n$ clusters according to eqn (1) provide useful experimental information about the binding energies assuming a simple model.[32,50] In this model, the absorbed photon energy ($h\nu_{IR}$) is available for the evaporation of the most weakly bound ligands in the cluster. Similar to related aromatic cluster systems,[32] IRPD of $TRA^+–(N_2)_n$ produces predominantly a single $TRA^+–(N_2)_m$ fragment channel, and they are indicated in Fig. 2. For clusters with $n \leq 4$, the resonant absorption of a photon with $h\nu_{IR} \sim$ 3400 cm^{-1} is sufficient to evaporate all N_2 ligands (m = 0), while for n = 5 and 6 only four ligands can be released (m = 1 and 2, respectively). These fragmentation channels are fully consistent with the binding energies calculated at the ωB97X-D/cc-pVTZ level, D_0(H) = 981 cm^{-1} for the first H-bound ligand (n = 1), $D_0(\pi)$ = 688 cm^{-1} for a π-bound ligand (n = 1), and $D_0(H^{2nd})$ = 669 cm^{-1} for the second H-bound ligand (n = 2). Neglecting three-body interactions and assuming that all π-bound ligands have essentially the same binding energy, the total binding energies of the most stable n = 1–6 clusters are estimated to be 981, 1650, 2338, 3026, 3714, and 4402 cm^{-1}, respectively. These binding energies predict for $n \leq 4$ a complete desolvation and the evaporation of four ligands for n = 5 and 6 upon IRPD at 3400 cm^{-1}. This agreement with experiment demonstrates that the theoretical level reliably predicts the binding energies of $TRA^+–(N_2)_n$ and that the clusters indeed absorb only a single IR photon.

3.4.3 Effects of ionization. Nonpolar ligands such as Ar and N_2 tend to form π-bound complexes with aromatic molecules in the S_0 electronic state, because the dispersion forces prefer π-bound geometries to H-bound structures. Unfortunately, there are no available experimental data for the structure of TRA–N_2 (as well as In–N_2) in the S_0 state. It has been established, however, that aromatic molecules with acidic NH groups such as aniline form π-bound complexes with N_2 in the S_0 state.[32] In addition, In forms a π-bound complex with Ar in the S_0 state, suggesting that the aromatic π-cloud of neutral TRA is the preferential binding site for the nonpolar N_2 ligand in the S_0 state. In the D_0 state of TRA^+, however, the indolic NH group is by far the preferential binding site for N_2, leading to $TRA^+–N_2$(H) as the most stable isomer. Therefore, ionization of TRA drastically changes the preferred intermolecular binding motif with nonpolar molecules. Such an ionization-induced switch of the binding sites of TRA suggests that the variation of the charge brings about some modifications for hydrophobic interactions, which then offers different schemes for molecular recognition in nonpolar environments.

3.4.4 Effects of the side chain. It is instructive to compare the properties of TRA^+–L clusters with those of In^+–L to evaluate the effect of the ethylamino side chain on the intermolecular interaction. To this end, Table 2 compares salient properties of the intermolecular NH–N_2 and intramolecular indolic N–H bonds of TRA^+–L(H) and In^+–L(H) with L = N_2 and H_2O.

Table 2 Salient parameters of the intermolecular NH–N_2 and intramolecular indolic N–H bonds of TRA^+–L and In^+–L with L = N_2 and H_2O, evaluated at the ωB97X-D/cc-pVTZ level

Parameter[a]	In^+	In^+–N_2(H)	In^+–N_2(π)	In^+–H_2O(H)	TRA^+	TRA^+–N_2(H)	TRA^+–N_2(π)[c]	TRA^+–H_2O(H)
R_{NH}/Å	1.00758	1.01315	1.00737	1.03029	1.00715	1.01206	1.00711	1.02785
ν_{NH}/cm^{-1}	3453	3366	3455	3077	3457	3379	3458	3126
I_{NH} /km mol^{-1}	186	671	181	1467	169	616	167	1396
$\Delta\nu_{NH}$/cm^{-1}		−87	2	−376		−78	1	−331
R/Å		2.13	3.68	1.74		2.16	3.93	1.75
ν_s/cm^{-1}		96	72	195		84	48	200
D_e[b]/kJ mol^{-1}		16.2 (1355)	9.9 (824)	70.4 (5889)		14.2 (1188)	9.6 (806)	64.7 (5405)
D_0[b]/kJ mol^{-1}		13.1 (1094)	7.1 (591)	63.1 (5271)		11.7 (981)	8.2 (688)	57.8 (4835)

[a] Intramolecular N–H bond length (R_{NH}), stretch frequency and IR intensity (ν_{NH}, I_{NH}); intermolecular NH–N_2 bond length (R), stretch frequency (ν_s), and binding energy ($D_{e/0}$). [b] Binding energies in cm^{-1} are listed in parentheses. [c] Data for TRA^+–$N_2(\pi_{top})$.

Apparently, the indolic N–H bond in TRA^+ (assuming to have the G*py*(in) conformation) is slightly stronger and shorter than in In^+, leading to a slightly larger ν_{NH} frequency. Thus, the side chain reduces the acidity of the NH group, as also indicated by the smaller positive partial charge on the NH proton (q_H = 0.439 and 0.443 *e* for TRA^+ and In^+, respectively). As a consequence of its smaller H-bonding proton donor ability, the intermolecular H-bonds in TRA^+–L(H) are slightly weaker and longer than in In^+–L(H). For example, the binding energies calculated for TRA^+–N_2(H) and TRA^+–H_2O(H) (981 and 4835 cm^{-1}) are lower than those of In^+–N_2(H) and In^+–H_2O(H) (1094 and 5271 cm^{-1}), respectively. As a consequence of the weaker interaction in TRA^+–L(H), the $\Delta\nu_{NH}$ redshifts are smaller than in In^+–L(H), in agreement with the experimental observation. The calculated binding energy of In^+–H_2O(H), D_0(H) = 5271 cm^{-1}, is close to the measured value, D_0(H) = 4790 ± 10 cm^{-1},[58] again indicating that the applied theoretical level reliably reproduces the intermolecular interaction of TRA^+/In^+ with polar and nonpolar ligands. The similar photofragmentation branching ratios observed for IRPD of TRA^+–$(N_2)_n$ and In^+–$(N_2)_n$ confirm that the side chain has only a modest impact on the intermolecular interaction of TRA^+ with nonpolar ligands, consistent with the similar binding energies predicted for both the H-bonded and π-bonded ligands of TRA^+–L and In^+–L.

4. Conclusions

IR photodissociation spectra of TRA^+–$(N_2)_n$ in the size range n = 1–6 have been measured in the vicinity of the indolic NH stretch fundamental (ν_{NH}) to investigate the weak H-bonding interaction of TRA^+ with nonpolar N_2 molecules. Two types of structural isomers were identified in the IRPD spectrum of the TRA^+–N_2 dimer (n = 1), namely the H-bound TRA^+–N_2(H) global minimum, in which N_2 forms a linear H-bond to the indolic NH group of TRA^+, and the significantly less stable π-bound TRA^+–N_2(π) local minima, in which N_2 is attached to the aromatic pyrrole ring of TRA^+. The ν_{NH} frequency redshift of TRA^+–N_2(H) is about 20% of that of TRA^+–H_2O(H), consistent with the formation of a much weaker σ H-bond in the former complex. The broad ν_{NH} band observed in the IRPD spectrum of TRA^+–$(N_2)_2$ is interpreted with the contribution of two stable isomers with roughly similar binding energies but different H-bonding configurations. The red side is assigned to the ν_{NH} mode of the H/π isomer, whereas the blue side is attributed to the 2H isomer. The ν_{NH} bands of larger TRA^+–$(N_2)_n$ clusters with n = 3–6 show only modest incremental blueshifts from ν_{NH} of the 2H isomer, indicating that the microsolvation proceeds by attaching weakly bound N_2 ligands to the central 2H core ion, which exhibits a planar bifurcated asymmetric H-bond configuration. Thus, at the cluster size n = 2, the preferred H-bonding motif in TRA^+–$(N_2)_n$ changes from singly H-bound structures (n = 1) to doubly H-bound structures ($n \geq 3$). Interestingly, the NBO analysis of TRA^+–$(N_2)_2$ reveals that the local H-bond strength between the indolic NH group and the N_2 molecule(s) is significantly smaller for the 2H isomer than for the H/π isomer. This result implies that not only the weak H-bonds to the nonpolar N_2 ligands in TRA^+–$(N_2)_n$ determine the total stability of the clusters but a subtle balance between various intermolecular interactions, including local H-bonds, charge–quadrupole and induction interactions, dispersion, and exchange repulsion, controls the total stability. The bifurcated binding motif in TRA^+–(N_2)(2H) with its unique spectroscopic signature (substantial incremental blueshift and red shaded band contour of the NH stretch fundamental) has previously been identified for In^+–$(N_2)_2$(2H) but not for other aromatic ions with NH and OH donors, such as aniline and phenol. Thus, it may be speculated that this binding motif is typical for heterocyclic aromatic cations featuring acidic NH donor groups. Indeed, inspection of the IR spectra of imidazole$^+$–$(N_2)_n$ clusters reported in ref. 43 also exhibits the spectroscopic signature of the bifurcated binding motif for $n \geq 2$ (although not identified as such in ref. 43), supporting this hypothesis.

Acknowledgements

This work was partly supported by TU Berlin, the Deutsche Forschungsgemeinschaft (DO 729/4), the German–Israeli Foundation (G.I.F. 1164-158.5/2011), the Grants in Aid for Young Scientists A (23685005) from the Ministry of Education, Sports, Science and Technology in Japan (MEXT), the JSPS Core-to-Core Program ''Photoionization-induced switch in aromatic molecule-solvent recognition'', and the Cooperative Research Program ''Network Joint Center for Materials and Devices''.

References

1 H. Lodish, A. Berk, P. Matsudaira, C. A. Kaiser, M. Krieger, M. P. Scott, L. Zipursky and J. W. H. Darnell, *Molecular cell biology*, Freeman & Co., 2004.
2 Y. Levy and J. N. Onuchic, *Annu. Rev. Biophys. Biomol. Struct.*, 2006, **35**, 389.
3 W. Kauzmann, *Adv. Protein Chem.*, 1959, **14**, 1.
4 D. Eisenberg and A. D. McLachlan, *Nature*, 1986, **319**, 199.
5 G. R. Desiraju and T. Steiner, *The weak hydrogen bond in structural chemistry and biology*, Oxford University Press, 2001.
6 K. Müller-Dethlefs, O. Dopfer and T. G. Wright, *Chem. Rev.*, 1994, **94**, 1845.
7 T. S. Zwier, *Annu. Rev. Phys. Chem.*, 1996, **47**, 205.
8 T. Ebata, A. Fujii and N. Mikami, *Int. Rev. Phys. Chem.*, 1998, **17**, 331.
9 B. Brutschy, *Chem. Rev.*, 2000, **100**, 3891.
10 C. Manca, C. Tanner and S. Leutwyler, *Int. Rev. Phys. Chem.*, 2005, **24**, 457.
11 H. Sekiya and K. Sakota, *J. Photochem. Photobiol., C*, 2008, **9**, 81.
12 Y. Matsuda, N. Mikami and A. Fujii, *Phys. Chem. Chem. Phys.*, 2009, **11**, 1279.
13 M. Fujii and O. Dopfer, *Int. Rev. Phys. Chem.*, 2012, **31**, 131.
14 E. J. Bieske and O. Dopfer, *Chem. Rev.*, 2000, **100**, 3963.
15 M. A. Duncan, *Int. Rev. Phys. Chem.*, 2003, **22**, 407.
16 W. H. Robertson and M. A. Johnson, *Annu. Rev. Phys. Chem.*, 2003, **54**, 173.
17 J. R. Carney and T. S. Zwier, *J. Phys. Chem. A*, 2000, **104**, 8677.
18 B. C. Dian, J. R. Clarkson and T. S. Zwier, *Science*, 2004, **303**, 1169.
19 L. A. Peteanu and D. H. Levy, *J. Phys. Chem.*, 1988, **92**, 6554.
20 N. Mayorkas, A. Bernat, S. Izbitski and I. Bar, *J. Chem. Phys.*, 2013, **138**, 124312.
21 Q. Gu and J. L. Knee, *J. Chem. Phys.*, 2012, **137**, 104312.
22 K. Sakota, Y. Kouno, S. Harada, M. Miyazaki, M. Fujii and H. Sekiya, *J. Chem. Phys.*, 2012, **137**, 224311.
23 L. A. Philips and D. H. Levy, *J. Chem. Phys.*, 1988, **89**, 85.
24 L. L. Connell, T. C. Corcoran, P. W. Joireman and P. M. Felker, *J. Phys. Chem.*, 1990, **94**, 1229.
25 N. Mayorkas, S. Izbitski, A. Bernat and I. Bar, *J. Phys. Chem. Lett.*, 2012, **3**, 603.
26 J. R. Carney and T. S. Zwier, *Chem. Phys. Lett.*, 2001, **341**, 77.
27 M. Schmitt, M. Böhm, C. Ratzer, C. Vu, I. Kalkman and W. L. Meerts, *J. Am. Chem. Soc.*, 2005, **127**, 10356.
28 J. R. Clarkson, B. C. Dian, L. Moriggi, A. DeFusco, V. McCarthy, K. D. Jordan and T. S. Zwier, *J. Chem. Phys.*, 2005, **122**, 214311.
29 J. R. Clarkson, J. M. Herbert and T. S. Zwier, *J. Chem. Phys.*, 2007, **126**, 134306.
30 M. Böhm, J. Tatchen, D. Krügler, K. Kleinermanns, M. G. D. Nix, T. A. LeGreve, T. S. Zwier and M. Schmitt, *J. Phys. Chem. A*, 2009, **113**, 2456.
31 J. L. Alonso, V. Cortijo, S. Mata, C. Perez, C. Cabezas, J. C. Lopez and W. Caminati, *J. Mol. Spectrosc.*, 2011, **269**, 41.
32 O. Dopfer, *Z. Phys. Chem.*, 2005, **219**, 125.
33 O. Dopfer, R. V. Olkhov and J. P. Maier, *J. Chem. Phys.*, 1999, **111**, 10754.
34 N. Solcà and O. Dopfer, *Chem.–Eur. J.*, 2003, **9**, 3154.
35 N. Solcà and O. Dopfer, *Chem. Phys. Lett.*, 2000, **325**, 354.
36 N. Solcà and O. Dopfer, *Chem. Phys. Lett.*, 2001, **342**, 191.
37 N. Solcà and O. Dopfer, *J. Phys. Chem. A*, 2001, **105**, 5637.
38 H.-S. Andrei, N. Solcà and O. Dopfer, *Phys. Chem. Chem. Phys.*, 2004, **6**, 3801.
39 N. Solcà and O. Dopfer, *J. Chem. Phys.*, 2004, **120**, 10470.
40 N. Solcà and O. Dopfer, *J. Phys. Chem. A*, 2002, **106**, 7261.
41 F. M. Pasker, N. Solcà and O. Dopfer, *J. Phys. Chem. A*, 2006, **110**, 12793.
42 M. Schmies, A. Patzer, S. Kruppe, M. Miyazaki, S. Ishiuchi, M. Fujii and O. Dopfer, *ChemPhysChem*, 2013, **14**, 728.
43 H.-S. Andrei, N. Solcà and O. Dopfer, *J. Phys. Chem. A*, 2005, **109**, 3598.
44 O. Dopfer, D. Roth and J. P. Maier, *J. Am. Chem. Soc.*, 2002, **124**, 494.
45 O. Dopfer, D. Roth and J. P. Maier, *Int. J. Mass Spectrom.*, 2002, **218**, 281.
46 N. Solcà and O. Dopfer, *Phys. Chem. Chem. Phys.*, 2004, **6**, 2732.
47 A. Lagutschenkov, J. Langer, G. Berden, J. Oomens and O. Dopfer, *J. Phys. Chem. A*, 2010, **114**, 13268.
48 A. Lagutschenkov, J. Langer, G. Berden, J. Oomens and O. Dopfer, *Phys. Chem. Chem. Phys.*, 2011, **13**, 2815.
49 A. Lagutschenkov, J. Langer, G. Berden, J. Oomens and O. Dopfer, *Phys. Chem. Chem. Phys.*, 2011, **13**, 15644.
50 O. Dopfer, *Int. Rev. Phys. Chem.*, 2003, **22**, 437.
51 C. Unterberg, A. Jansen and M. Gerhards, *J. Chem. Phys.*, 2000, **113**, 7945.
52 M. J. Frisch, G. W. Trucks, H. B. Schlegel, G. E. Scuseria, M. A. Robb, J. R. Cheeseman, G. Scalmani, V. Barone, B. Mennucci, G. A. Petersson, H. Nakatsuji, M. Caricato, X. Li, H. P. Hratchian, A. F. Izmaylov, J. Bloino, G. Zheng, J. L. Sonnenberg, M. Hada, M. Ehara, K. Toyota, R. Fukuda, J. Hasegawa, M. Ishida, T. Nakajima, Y. Honda, O. Kitao, H. Nakai, T. Vreven, J. A. Montgomery Jr, J. E. Peralta, F. Ogliaro, M. Bearpark, J. J. Heyd, E. Brothers, K. N. Kudin, V. N. Staroverov, R. Kobayashi, J. Normand, K. Raghavachari, A. Rendell, J. C. Burant, S. S. Iyengar, J. Tomasi, M. Cossi, N. Rega, J. M. Millam, M. Klene, J. E. Knox, J. B. Cross, V. Bakken, C. Adamo, J. Jaramillo, R. Gomperts, R. E. Stratmann, O. Yazyev, A. J. Austin, R. Cammi, C. Pomelli, J. W. Ochterski, R. L. Martin, K. Morokuma, V. G. Zakrzewski, G. A. Voth, P. Salvador, J. J. Dannenberg, S. Dapprich, A. D. Daniels, Ö. Farkas, J. B. Foresman, J. V. Ortiz, J. Cioslowski and D. J. Fox, *Gaussian 09, Revision A.01*, Gaussian, Inc., Wallingford CT, 2009.
53 R. V. Olkhov and O. Dopfer, *Chem. Phys. Lett.*, 1999, **314**, 215.
54 O. Dopfer, D. Roth, R. V. Olkhov and J. P. Maier, *J. Chem. Phys.*, 1999, **110**, 11911.
55 O. Dopfer, D. Roth and J. P. Maier, *J. Phys. Chem. A*, 2000, **104**, 11702.
56 A. E. Reed, L. A. Curtiss and F. Weinhold, *Chem. Rev.*, 1988, **88**, 899.
57 F. Weinhold and C. R. Landis, *Valency and Bonding*, Cambridge University Press, 2005.
58 J. E. Braun, T. Mehnert and H. J. Neusser, *Int. J. Mass Spectrom.*, 2000, **203**, 1.

